



Article

Development of an Autonomous Driving Path-Generation Algorithm for a Crawler-Type Ridge-Forming Robot

Joong-hee Han D and Chi-ho Park *

Division of AI, Big Data and Block Chain, Daegu Gyeongbuk Institute of Science and Technology (DGIST), Daegu 42988, Republic of Korea; jhhan@dgist.ac.kr

* Correspondence: chpark@dgist.ac.kr; Tel.: +82-53-785-4441

Abstract: The agricultural sector is currently facing problems including a decline in the agricultural population, labor shortages, and an aging population. To solve these problems and increase agricultural productivity, the development and distribution of autonomous agricultural machinery is necessary. Since autonomous agricultural machinery is operated along a pre-defined path, it is essential to generate an autonomous driving path that takes into account the driving and working methods of the agricultural machinery. In this study, an autonomous driving path-generation algorithm for the autonomous operation of a crawler-type ridge-forming robot is proposed. The proposed algorithm defines the field boundary using the geodetic coordinates of the field boundary points and the size of the robot, generates working line segments within the field boundary, and generates three types of waypoints, which constitute an autonomous driving path based on the autonomous driving operating scenario. To verify the proposed algorithm, tests were conducted using four types of field boundary points with different shapes, and the results are presented. As a result of the simulation test, when a ridge was created using the generated autonomous driving path, the area occupied by the ridge in the total field area according to the field types of a rectangle, trapezoid, pentagon, and hexagon was indicated to be 80, 77, 85, and 77%, respectively.

Keywords: autonomous driving path generation; waypoints; ridge-forming robot



Academic Editor: Alessandro Gasparetto

Received: 1 November 2024 Revised: 3 January 2025 Accepted: 17 January 2025 Published: 20 January 2025

Citation: Han, J.-h.; Park, C.-h.
Development of an Autonomous
Driving Path-Generation Algorithm
for a Crawler-Type Ridge-Forming
Robot. *Appl. Sci.* 2025, 15, 987.
https://doi.org/10.3390/
app15020987

Copyright: © 2025 by the authors. Licensee MDPI, Basel, Switzerland. This article is an open access article distributed under the terms and conditions of the Creative Commons Attribution (CC BY) license (https://creativecommons.org/licenses/by/4.0/).

1. Introduction

One of the challenges facing modern agriculture is the falling income rates of farmers due to labor shortages and rising labor costs. One of the most labor-intensive tasks in field farming is ridge formation, and considering the rising labor costs, there is interest in new technology that can replace labor. Autonomous driving technology for agricultural machinery is being actively developed for this purpose, using ICT technology and advanced sensors. Such systems are expected to help address problems in the agricultural sector, such as a declining farm population, labor shortages, and food shortages. Global agricultural machinery companies such as John Deere, CNH Industrial, and Yanmar have launched autonomous tractors that combine sensors such as GNSS, cameras, and lidar with AI [1].

Since autonomous agricultural machinery driving is performed along a pre-defined path, generating the autonomous driving path is essential for autonomous operation. In addition, the cultivation rate and efficiency also depend on path generation, so the path generation must be designed to match the driving and working methods of the agricultural machinery. For this reason, much research has been conducted on path-generating methods for autonomous agricultural machinery. Current methods for generating autonomous

driving paths can be divided into those that use location data obtained by driving the route in advance [2–4] and methods that employ a geometric map [5–10]. The location data method obtained by driving a path in advance has the advantage of being relatively simple to execute, and creates a driving path that considers the positions and rotation spaces of surrounding obstacles. For example, Unal and Topakci [2] defined an autonomous driving path by saving the location coordinates obtained by driving the route manually as waypoints. Han et al. [3] generated an autonomous driving path by extracting essential waypoints required for autonomous driving based on the location data for the route acquired through manual driving, the intervals between waypoints, and the angles of straight lines generated by adjacent waypoints. Han et al. [4] proposed a method to obtain location data for individual passages in an orchard, merge them to create an orchard map, and then generate an autonomous driving route based on this. However, it takes a lot of time and labor to create a route over a large area, and there is a disadvantage in that it is difficult to change the driving pattern according to the work method. Therefore, the above method is best suited for fruit farming, such as orchards, where permanent obstacles exist and the same work is performed each time.

The geometric map method defines a space in which the autonomous work can be performed using objects made up of points and lines, and it generates a path which considers the rotation and working methods of the agricultural machinery. For example, Palmer et al. [5] suggested a method that generated predetermined efficient courses using a field map to reduce overlapping and missed courses. Taïx et al. [6] proposed an algorithm based on the treatment of convex cells and the definition of characteristic points to generate field-work tracks in the polygonal fields. Oksanen and Visala [7] presented an algorithm to solve coverage path planning using a geometric map. This algorithm splits a complexshaped field into simple trapezoid fields and generates straight field-work tracks. Hameed et al. [8] presented a method for the generation of a geometric field representation to provide a map, on which the operational planning of field operations could be carried out. Hameed et al. [9] developed a 3D coverage algorithm where 2D coverage paths are projected through the field terrain. Luck et al. [10] introduces the automatic boom section control technology based on a map. The advantage of using geometric maps is that autonomous driving routes can be generated regardless of the shape of the field or the working method. However, a precise and high-resolution geometric map must be built in advance, and the more complex the shape of the field, the more difficult it can be to generate a path. The method of using a geometric map is mainly used to generate autonomous paths for agricultural machinery used in upland fields or rice paddies.

Typically, the shape of a field is a simple polygon, and there are usually no obstacles inside. In other words, the geometric map of the field can be simply expressed as the coordinates of the boundary points that make up the boundary of the field. Therefore, studies have been conducted to generate autonomous driving paths using the coordinates of field boundary points. Jeon et al. [11] inputted the coordinates of the field boundary points, converted them into a grid map, and researched generating a path based on the shortest distance using the A* algorithm for an autonomous tractor in a paddy field. This method has the disadvantage that the location accuracy of the generated waypoints may vary depending on the resolution of the grid map, and that the higher the resolution, the greater the computational amount. Han et al. [12] developed an infield route-planning program that can generate an X-type turning, pattern-based coverage path map that provides guidance lines for autonomous tillage tractors in the polygonal field based on inputted boundary points. Jeon et al. [13] generated an autonomous puddling and leveling tractor path by inputting the coordinates of field boundary points, generating interwork tracks, and applying a genetic algorithm to determine the work order of the interwork

Appl. Sci. 2025, 15, 987 3 of 20

tracks that minimizes the headland turning distance. The above two studies are suitable for generating autonomous driving paths for wheeled agricultural machines such as tractors, but are inefficient for application to crawler-type agricultural machines capable of turning in place because they set unnecessary turning sections.

In order to obtain the coordinates of the field boundary points, it is essential to obtain coordinates through surveying. However, since surveying requires manpower and costs, studies have also been conducted to generate an autonomous driving route by obtaining two reference points inside the field or obtaining boundary points from Google Maps. Lee et al. [14] propose a method to generate the autonomous driving path of the harvester which defines two reference points inside the field to create a path, creates a straight work line by moving the straight line created as the reference point in parallel by the width of the work machine, and then applies the alpha turn method to create the autonomous driving path. In the above method, if the positions of the two reference points inside the field are incorrectly designated, the working straight lines generated through parallel movement may not include all of the inside of the field. Crisnapati and Maneetham [15] presented a two-dimensional path planning platform using an edge-vertex path algorithm based on Laravel and Google Maps for the Autonomous Walk-Behind Hand Tractor. This algorithm automatically generates a route by considering the boundaries on the map, the distance between the routes, and the start and end points. However, due to the limitations of the map's location accuracy, the generated route is made up of location data with a large error, and thus has limitations in being applied to actual autonomous driving.

In this paper, an autonomous driving path-generation algorithm for a crawler-type ridge-forming robot will be presented. Most current field farming already uses machines, so the shape of the fields is simple, and a crawler-type robot has the advantage of not having to consider rotation methods because they can rotate in place. In addition, since the shape of the field is simple, the geometric boundary of the field can be easily defined by obtaining the location data of the field boundary points through GNSS surveying. Therefore, for the autonomous operation of agricultural machinery, the proposed algorithm generates waypoints based on the absolute position using the geodetic coordinates of field boundary points measured with positioning sensors such as GNSS. The main contributions of this paper are as follows: (1) propose a path-generation algorithm for crawler-type agricultural machinery rather than wheeled agricultural machinery such as tractors; (2) generate an autonomous driving path covering the entire field using a simple mathematical method using only the coordinates of the field boundary points and the sizes of the robot and implement; and (3) generate waypoints step by step based on the defined autonomous driving ridge-forming operation scenario.

The structure of this paper is as follows. Section 2 introduces the proposed algorithm that generates an autonomous driving path for a ridge-forming robot by defining field boundaries, generating working line segments according to the field boundaries, and generating waypoints using the working line segments according to autonomous driving operation scenarios. Section 3 presents the test results of the proposed algorithm. Section 4 describes the discussion and conclusions.

2. Autonomous Driving Path-Generation Algorithm for a Ridge-Forming Robot

2.1. Overview of Autonomous Driving Path-Generation Algorithm

To operate the autonomous crawler-type ridge-forming robot in the field, an autonomous driving path must be generated that considers the driving and work to be performed within the field. The autonomous driving path can be expressed using way-points including the point type, location coordinates, and the task of the ridge-forming

Appl. Sci. **2025**, 15, 987 4 of 20

robot at the waypoint. To generate waypoints for the operation of the autonomous ridge-forming robot, an autonomous path-generation algorithm was developed consisting of four steps: the parameters input, field boundary definition, work-path generation, and waypoints' generation, as shown in Figure 1. Since the driving speed of the ridge-forming robot is very low, at a maximum of 4 km/h, meaning the robot dynamics are hardly affected during driving control, the proposed algorithm was developed to generate an autonomous driving path using a geometric method without considering the dynamic model.

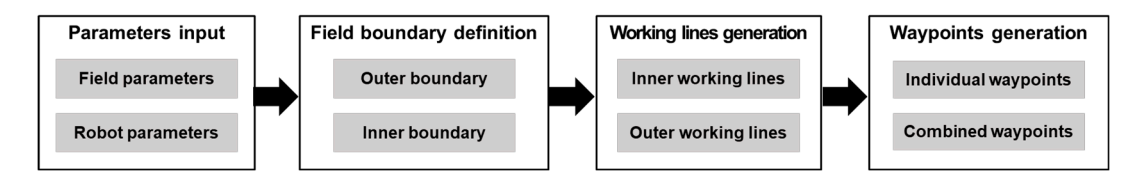


Figure 1. Process for the autonomous driving path generation.

2.2. Autonomous Driving Path-Generation Algorithm

2.2.1. Parameter Input

The first step in the autonomous driving path-generation algorithm is to input parameters about the field and the ridge-forming robot. The field parameters are the geodetic coordinates (latitude, longitude, and ellipsoidal height) of the vertices that make up the field boundary. The geodetic coordinates of the vertices constituting the field boundary can be obtained from GNSS surveying or maps. The obtained geodetic coordinates must have a precision of 5 cm to ensure autonomous driving accuracy. The geodetic coordinates of the vertices are entered sequentially clockwise, starting from the vertex of the field boundary closest to the field entrance. The parameters of the ridge-forming robot consist of the specifications of the ridge-forming robot and the ridge-forming working information. The parameters for the specifications of the ridge-forming robot are the size of the robot and the agricultural implement, and the width of the ridge.

2.2.2. Field Boundary Definition

The second step in the autonomous driving path-generation algorithm is to define the outer- and the inner-field boundary, to set the inner work area and the headland area. The method used to define the outer- and the inner-field boundary in this study is to calculate the north-east-down (NED) coordinates of the vertices of the boundary and the parameters of the equation of a straight line of the boundary lines. For this, first, since the inputted field parameters which are the coordinates of the vertices constituting the field boundary are geodetic coordinates on an ellipsoid, they are converted to NED coordinates based on the coordinates of the first field boundary point, to convert them to coordinates on a plane. After completing the coordinate transformation, starting from the first point of the input field boundary, the two points of the line segment constituting the field in a clockwise direction and the calculated slope (*m*) and y-intercept (*c*) of the straight line are defined, which are the parameters of the equation of a straight line. When calculating the parameters of the equation of a straight line, the x and y axes are, respectively, the same as the east and north axes in the NED coordinate system. The NED coordinates of the vertices of the outer boundary and the parameters of the equation of the straight line for the line segments constituting the outer boundary are stored.

The inner boundary of the field is the inner work area of the field and is defined by excluding the headland area, which is the area where the robot turns from the area created as the external boundary of the field. The internal border and boundary points of the field are created by calculating the equation of a straight line, that is, the width of the headland area (*d*) away from the external border of the field, and then calculating the intersection

point using the straight-line equation. Since the ridge-forming robot used in this study is a crawler-type robot, the rotation method in the headland area is set for in situ rotation to expand the ridge-forming area. Thus, the width of the headland area is defined as the sum of the length of the robot and the agricultural implement.

The coordinates of the vertices of the inner-field boundary are defined by calculating the intersection between adjacent inner boundary lines after calculating the equation of the straight line of the internal boundary, separated by the width of the headland area from each external boundary line constituting the outer-field boundary. The process of calculating the equation of the straight line of the internal boundary line that is the width of the headland area away from the external boundary line to define the internal boundary line and boundary point is as follows.

First, two internal boundary candidate lines are created that are the same as the slope of the external boundary line, and are separated by the width of the headland area in the direction orthogonal to the external boundary line, as illustrated in Figure 2a. The slope of the equation of the straight line of the created two internal boundary candidate lines is the same as the slope of the straight line of the external boundary line (m_i), and the y-intercept of the two created internal boundary candidate lines is calculated by:

$$b_{i,1} = b_i + d_h \times \sqrt{m_i^2 + 1}$$

$$b_{i,2} = b_i - d_h \times \sqrt{m_i^2 + 1}$$
(1)

where $b_{i,1}$ and $b_{i,2}$ are the y-intercept of the two created internal boundary candidate lines, b_i is the y-intercept of the straight line of the outer boundary line, d_h is the width of the headland area, and m_i is the slope of the straight line of the outer boundary line.

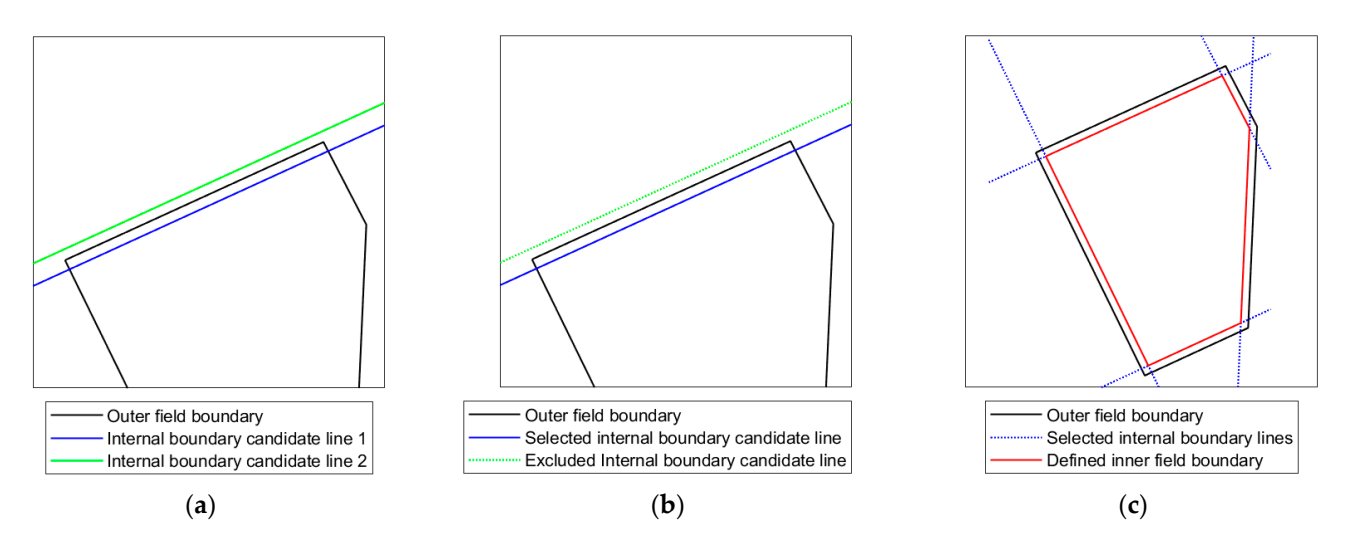


Figure 2. Process of defining the inner-field boundary: (a) creating two internal boundary candidate lines; (b) internal boundary candidate line selection; (c) inner-field boundary definition.

Next, among the two internal boundary candidate lines, the internal boundary line that passes through the interior of the external boundary of the field is selected, as illustrated in Figure 2b. To do this, the intersection of two external boundary lines connected to the currently selected external boundary line and the two internal boundary candidate lines are calculated. And, when intersections are contained in two external boundary lines connected to the currently selected external boundary line, the slope and y-intercept of the internal boundary line used in the calculation of the intersection points are saved. When the calculation of the slope and y-intercept of the internal boundary line for each external boundary line is completed, the intersection between the adjacent internal boundary lines

is calculated and defined as the coordinates of the vertices of the inner-field boundary, as illustrated in Figure 2c.

2.2.3. Working-Line Generation

The working line refers to a set of line segments in which ridge-forming work is performed. It is generated in the inner-field boundary and the headland area, respectively. The process of generating the working line in the inner-field boundary consists of four steps: the definition of a minimum bounding rectangle (MBR), the generation of candidate sets consisting of line segments within the MBR, the generation of candidate sets consisting of line segments within the inner-field boundary, and the final selection of a set of line segments.

The first step is to produce an MBR, which is a rectangle of the minimum area including the set of the vertices of the inner-field boundary. Since this study generates line segments on the plane, the MBR of the inner-field boundary is defined as using the minimum North coordinate ($\min[B_{i,north}^I]$), the maximum North coordinate ($\max[B_{i,north}^I]$), the minimum East coordinate ($\min[B_{i,east}^I]$), and the maximum East coordinate ($\max[B_{i,east}^I]$) among the coordinates of the vertices of the inner-field boundary. The coordinate of the vertices of the MBR of the inner-field boundary (B^M) is defined by:

$$\boldsymbol{B}^{M} = \begin{bmatrix} \min[B_{i,north}^{I}] & \min[B_{i,east}^{I}] \\ \max[B_{i,north}^{I}] & \min[B_{i,east}^{I}] \\ \max[B_{i,north}^{I}] & \max[B_{i,east}^{I}] \\ \min[B_{i,north}^{I}] & \max[B_{i,east}^{I}] \end{bmatrix}$$
(2)

For the second step, candidate sets consisting of line segments within the MBR are generated according to the slope of the line segment by considering the slope angle of the line segments of the inner-field boundary, since the line segment may be generated in various directions according to the shape of the field boundary. The method for generating candidate sets consisting of line segments within the MBR is as follows.

First, the nearest vertex to the origin of the NED coordinate system among the vertices of the MBR of the inner-field boundary is selected. Then the slope angle is calculated for each of the two-line segments of the MBR including the MBR vertex nearest to the origin of the NED coordinate system. The calculated slope angle for each of the two-line segments of the MBR is the maximum and minimum range of the slope angle used to generate work line segments, and a set of slope angles is defined at one-degree intervals within the range of the slope angles. For each of the generated slope angles, the slope and y-intercept for the straight-line candidates are calculated according to the slope angle as follows.

1. The slope of the straight line is defined using the slope angle as:

$$m_i = \tan \alpha_i \tag{3}$$

where m_i is the slope of the straight line according to the *i*-th slope angle and α_i is the *i*-th slope angle.

2. The y-intercept (c_0) of the straight line with the slope (m_i) and passing through the MBR vertex nearest to the origin of the NED coordinate system is calculated by:

$$c_0 = -m_i B_{o,east}^I + B_{o,north}^I \tag{4}$$

where $B_{o,north}^{I}$ and $B_{o,east}^{I}$ are the North and East coordinates of the MBR vertex nearest to the origin of the NED coordinate system.

3. A straight line with the slope (m_i) is generated by increasing the y-intercept (c_j) of the straight line in a positive direction by the width of the ridge (d_r) . If there are two intersections between the straight line and the MBR boundary, the slope and y-intercept for the straight line are stored. The increments in the positive direction are repeated until two intersections no longer appear with the MBR boundary.

$$c_j = c_0 + d_r \times j \times \sqrt{m_i^2 + 1} \tag{5}$$

where j is a value that starts from 0 and increases by 1 until two intersections no longer appear within the MBR boundary.

4. Using the above equation, a straight line is generated in a negative direction by the width of the ridge, and if there are two intersections between the straight line and the MBR boundary, the slope and y-intercept for the straight line are stored. In the above equation, j is a value that starts from -1 and increases by -1; if two intersections do not appear, the above process is repeated for the next slope angle.

The third step is to generate candidate sets consisting of work line segments that meet the inner-field boundary, using a set of the slopes and y-intercepts of straight lines intersecting the MBR boundary for each slope angle of the straight line. If there are two intersections between the inner boundary and the straight line and the distance of the intersection is longer than twice the length of the ridge-forming robot, the coordinates of the intersection are stored as the coordinates of the two endpoints of the working line segment candidates.

The last step for the work path generation in the inner-field boundary is to select one working line segment group from among the working line segment candidate groups generated for each slope angle. To maximize the ridge-forming area, the total distance of the working line segment candidate groups generated for each slope angle is calculated, and the working line segment candidate group with the longest total distance is selected as the final inner working line segments in the inner-field boundary.

The method of generating outer working line segments within the headland area is as follows. The outer working line segments within the headland area are generated sequentially clockwise along the field boundary starting from the vicinity of the first vertex of the input field boundary points. Therefore, first, in the same way as the method of defining the inner-field boundary, outer working line segments that are half of the width of the headland area away from the external border of the field are created. Next, the length of the outer working line segments is adjusted considering the size of the robot so that the robot can move to a nearby outer working line segment within the headland area by rotating in place.

2.2.4. Waypoints Generation

In this step, autonomous driving paths for ridge-forming work are generated according to autonomous driving operation scenarios using the inner and outer working line segments generated in the working line generation step. An autonomous driving path is a series of waypoints that are sequential points to which the robot must drive, and location coordinates and work methods at those waypoints are described. In this study, the information included in a waypoint included a waypoint number, waypoint coordinates (latitude, longitude), and waypoint type. The waypoint type is defined by dividing it into a starting waypoint, straight waypoint, turning waypoint, work-starting waypoint, work-ending waypoint, and ending waypoint, considering the operation of a ridge-forming robot. In this study the autonomous driving scenarios for an autonomous crawler-type ridge-forming robot were divided into three types: autonomous ridge-forming in the inner field, autonomous driving

for returning to the starting point, and autonomous ridge-forming in the headland area. Therefore, the proposed algorithm generates waypoints corresponding to each autonomous driving scenario.

The first autonomous driving scenario, autonomous ridge-forming in the inner field, starts from the endpoint of the inner working line segment, which is the nearest to the coordinates of the first outer-field boundary point, and sequentially drives along the inner working line segments that are near to each other, to perform autonomous ridge-forming work. The method of generating waypoints for the scenario of autonomous ridge-forming in the inner field is as follows.

To define the reference point for generating waypoints, the inner working line segment closest to the first outer-field boundary point is extracted. Then, among the two endpoints of the extracted inner working line, the endpoint nearest to the first outer-field boundary point is defined as the reference point. Next, the distance between each inner working line segment and the reference point is calculated and the inner working line segments are sorted in order of the closest distance to the reference point.

To be sure the shortest distance is driven via all inner working line segments starting from the reference point, the two endpoints of each inner working line segment are defined as the starting or ending point, respectively. Next, four waypoints for each inner working segment are created by using the coordinates of the two endpoints of each inner working line segment, the length of the robot driving platform, and the length of the attached implement, considering the driving and working operations. The four waypoints created for each inner working segment are a waypoint located outside the inner boundary of the field to move to the waypoint that starts the ridge-forming operation, a waypoint to start the ridge-forming operation, a waypoint to end the ridge-forming operation, and a waypoint to move to the next inner working line. The coordinates of the waypoint are calculated to be located outside the starting point of the inner working line segment using the length of the inner working line segment and the length of the robot using the external section formula. The coordinates of the waypoint are calculated using the following formula, where m_e and n_e , which are the ratio values in the external section formula, are set as the length of the robot and the sum of the length of the robot and the length of the inner working line segment, respectively.

$$P(x_e, y_e) = \left(\frac{m_e x_2 - n_e x_1}{m_e - n_e}, \frac{m_e y_2 - n_e y_1}{m_e - n_e}\right)$$
(6)

where (x_e, y_e) are the coordinates of the external dividing point, (x_1, y_1) are the coordinates of the starting point of the inner working line segment, (x_2, y_2) are the coordinates of the ending point of the inner working line segment, and m_e and n_e are the ratio values in which the external dividing point divides the line externally.

The implement is attached to the rear of the robot driving platform and the inner working line is where the ridge is formed, so a waypoint to start the ridge-forming operation is located on or within the inner working line. Therefore, the coordinates of the waypoint to start the ridge-forming operation are calculated using the following internal section formula, with m_i and n_i , which are the ratio values in the internal section formula, set to the sum of the half-length of the robot and the length of the implement and the length of the inner working line segment minus the sum of the half-length of the robot and the length of the implement, respectively.

$$P(x_i, y_i) = \left(\frac{m_i x_2 + n_i x_1}{m_i + n_i}, \frac{m_i y_2 + n_i y_1}{m_i - n_i}\right)$$
(7)

where (x_i, y_i) are the coordinates of the internal dividing point, (x_1, y_1) are the coordinates of the starting point of the inner working line segment, (x_2, y_2) are the coordinates of the ending point of the inner working line segment, and m_i and n_i are the ratio values at which the internal dividing point divides the line internally.

The waypoint to end the ridge-forming operation, when the operation for the ridge-forming line is completed, is located outside of the ending point of the inner working line segments. The coordinates of the waypoint to end the ridge-forming operation are calculated using Equation (7) by setting the ratio values m_e and n_e to the sum of the half-length of the robot, the length of the implement, and the length of the inner working line segment as well as the sum of the half-length of the robot and the length of the implement.

A waypoint to move to the next inner working line is a point where the robot rotates in place to move near the next straight line. When rotating in place, track slip may occur, so taking this into account, the coordinates of the waypoint are calculated to be offset a certain way away from the waypoint to end the ridge-forming operation. The method for calculating the coordinates of a waypoint to move to the next inner working line is the same as that for a waypoint to end the ridge-forming operation, but the ratio values are set by adding an offset to the ratio values defined when calculating the coordinates of a waypoint to end the ridge-forming operation. However, for the last inner working line segment, the coordinates of a waypoint to move to the next inner working line are not calculated.

Once the task of creating four waypoints for each inner working line segment is completed, the coordinates of all waypoints expressed in the NED coordinate system are converted to geodetic coordinates. Then the geodetic coordinates of the waypoints are stored sequentially in the order in which the coordinates of the waypoints were calculated. The waypoint types of all generated waypoints are defined as follows.

The type of waypoint located outside the inner boundary of the field in order to move to the waypoint for starting the ridge-forming operation of the first inner working line segment is set as the starting point. The type of waypoint located outside the inner boundary of the field in order to move to the waypoint for starting the ridge-forming operation of the other inner working line segment is set as a turning point. The type of a waypoint to start the ridge-forming operation and a waypoint to end the ridge-forming operation of all the inner working line segments are set as the work-starting point and the work-ending point, respectively. The type of waypoint to move to the next inner working line is set as a turning point. Since the currently saved waypoint has no ending point, the type of waypoint to end the ridge-forming operation of the last inner working line segments is reset to the ending point.

The second autonomous driving scenario, autonomous driving for returning to the starting point in the headland area, starts from the last waypoint for autonomous ridge-forming in the inner field and sequentially drives along the outer working line segments to arrive at the endpoint of the outer working line segment nearest to the first outer-field boundary point. To create waypoints corresponding to the second autonomous driving scenario, first of all, the outer working line segment with the nearest distance from the last waypoint for autonomous ridge-forming in the inner field is selected, and the coordinates of a point within the selected line segment with the shortest distance from the last waypoint for autonomous ridge-forming in the inner field are calculated. And the coordinates of the last waypoint for autonomous ridge-forming in the inner field and the coordinates of a point within the selected line segment with the shortest distance are stored on waypoints.

Since the endpoints of the outer working line segments are connected, the total distance for each direction of rotation is calculated by moving clockwise and counterclockwise from the point within the selected line segment with the shortest distance from the last waypoint for autonomous ridge-forming in the inner field to the endpoint of the outer working line

segment nearest to the first outer-field boundary point, respectively. A list of a series of points consisting of an endpoint of outer working line segments moving to the starting point with the shortest distance is extracted, and the coordinates are stored in waypoints. The coordinates of all waypoints for the second autonomous driving scenario expressed in the NED coordinate system are converted to geodetic coordinates. The waypoint type for the first scenario and the waypoints are specified as the starting point and ending point, respectively. All waypoints except the first and last waypoints are points where the robot changes driving direction, so the waypoint type is set to turning waypoints.

The third autonomous driving scenario, autonomous ridge-forming in the headland area, starts from the endpoint of the outer working line segments, which is the nearest to the coordinates of the first outer-field boundary point, and sequentially drives along the outer working line segments that are near to each other to perform autonomous ridge-forming work. Since the outer working line segments are connected, we find the endpoint of the outer working line segments nearest the first outer-field boundary point, and then arrange the outer working line segments so that they can be connected sequentially in a clockwise direction.

Next, the endpoints of each outer working line segment are defined as the starting or ending points. For each outer working line segment, the following are defined: a waypoint located outside the inner boundary of the field to move to the waypoint of starting the ridge-forming operation; a waypoint to start the ridge-forming operation; a waypoint to end the ridge-forming operation; and a waypoint to move to the next inner working line and calculate their coordinates. Each outer working line segment's starting and ending points are set to a waypoint to start the ridge-forming operation and a waypoint to move to the next inner working line, respectively. The coordinates of a waypoint to start the ridge-forming operation, and a waypoint to end the ridge-forming operation for each outer working line segment, are calculated using Equation (7).

The ratio values (x_i, y_i) for calculating the waypoint to start the ridge-forming operation are the sum of the half-length of the robot and the length of the implement and the length of the outer working line segment minus the sum of the half-length of the robot and the length of the implement, respectively. In addition, the ratio values (x_i, y_i) for calculating the waypoint to end the ridge-forming operation are the length of the outer working line segment minus the sum of the half-length of the robot and the length of the implement and the sum of the half-length of the robot and the length of the implement, respectively. The type and coordinates of waypoints are defined, calculated, and saved in the same way as those using inner working line segments.

3. Results

3.1. Test Description

To verify the proposed algorithm, this study conducted an autonomous driving path generation test based on four types of fields with different shapes. The shapes of the fields used in the test were a rectangle, trapezoid, pentagon, and hexagon. Using Google Earth, field boundaries were defined according to their shape and vertex coordinates were obtained. The boundaries of the four types of fields defined by Google Earth are shown in Figure 3. The parameters to be input when generating the path, which are the length of the robot, the length of the agricultural implement, the width of the ridge, and the position error, were set to 3.0 m, 0.5 m, 1.2 m, and 0.1 m, respectively.

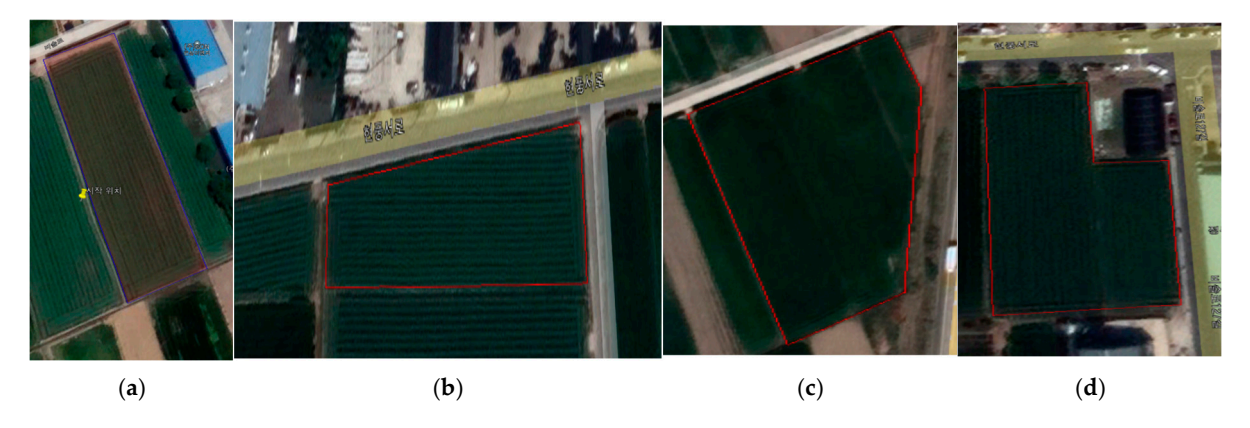


Figure 3. Boundaries of the four types of fields used in the experiment (red lines) obtained from Google Earth: (a) rectangle-shaped field; (b) trapezoid-shaped field; (c) pentagon-shaped field; (d) hexagon-shaped field.

3.2. Test Results

3.2.1. Rectangle-Shaped Field

The geodetic coordinates of the rectangle-shaped field boundary points for the test were entered clockwise from the northwest corner. The lengths of the four-line segments of the outer boundary of the field are approximately 36 m, 104 m, 36 m, and 104 m clockwise from the first input point, respectively, and the area is approximately 3741 m². The result of generating the inner boundary of the field using the coordinates of the input external boundary vertices is shown in Figure 4a. The short- and long-line segments of the inner boundary were approximately 98 m and 30 m, respectively, and the inner boundary was generated considering the length of the robot, so that the robot could rotate in place. Figure 4b shows the generated MBR of the internal boundary used to generate candidate sets consisting of line segments within the MBR.

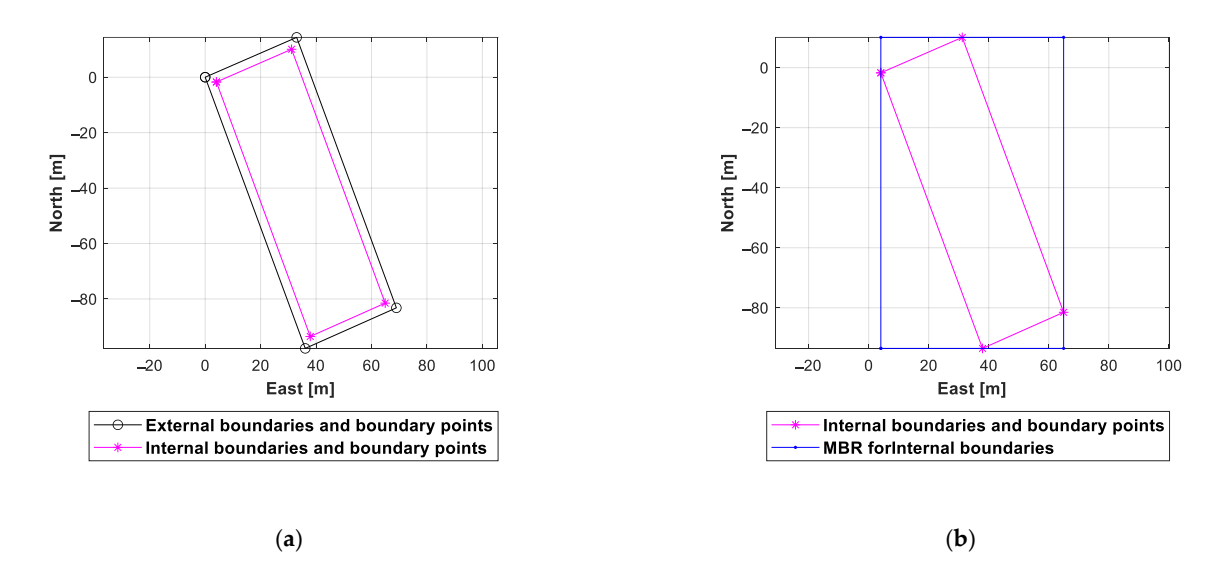


Figure 4. External and internal boundaries and MBR for the rectangle-shaped field: (a) External and internal boundaries; (b) internal boundaries and MBR for internal boundaries.

The results of the generated working line segments in the inner-field boundary and the headland area are shown in Figure 5a and Figure 5b, respectively. The number of generated working line segments in the inner-field boundary is 23. The range of the lengths of the generated working line segments in the inner-field boundary is 97.6 m to 97.8 m, and the sum of the generated working line segments in the inner-field boundary is 2247.9 m.

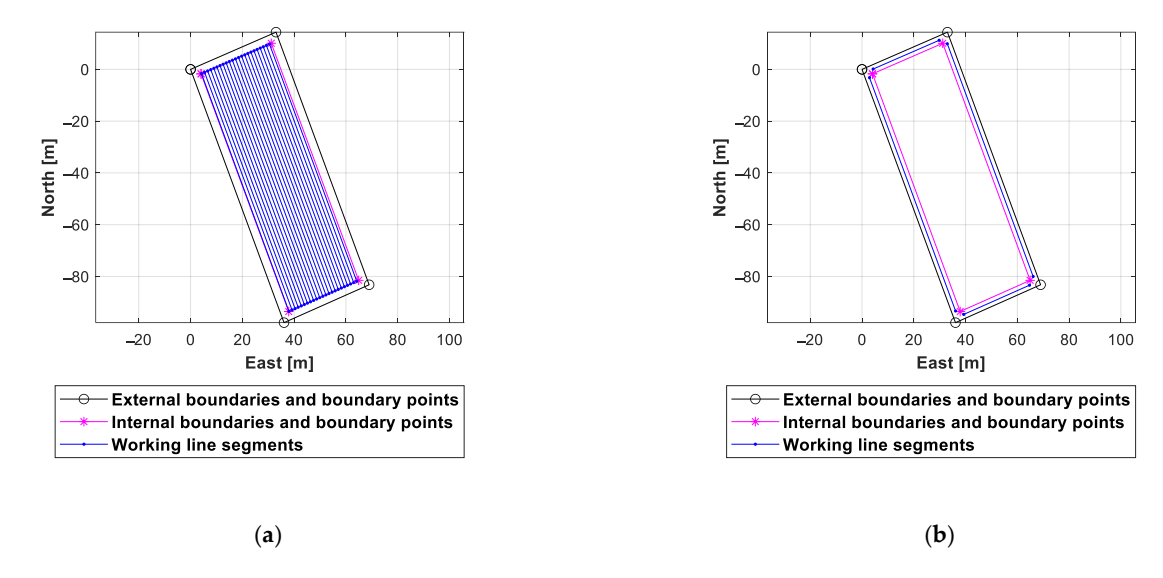


Figure 5. Working line segments for the rectangle-shaped field: (a) working line segments in the inner-field boundary; (b) working line segments in the headland area.

A total of four working line segments in the headland area were generated along the field boundaries. The range of the lengths of the generated working line segments in the headland area is 27.8 m to 96.1 m, and the sum of the generated working line segments in the headland area is 247.4 m. The total area of the ridges created through the working line segments is 2994 m^2 , so 80% of the field area is created as ridges.

For autonomous ridge-forming in the inner field, the results of the generated way-points are shown in Figure 6a. Waypoints were generated sequentially along the working line segments of the inner field that are closest in distance, starting near the first outer-field boundary point. A total of 91 waypoints were generated for autonomous ridge-forming in the inner field, and depending on the waypoint type, 1 starting waypoint, 44 turning waypoints, 23 work-starting waypoints, and 23 work-ending waypoints were generated. The total length of the autonomous driving path consisting of waypoints is 5433.8 m.

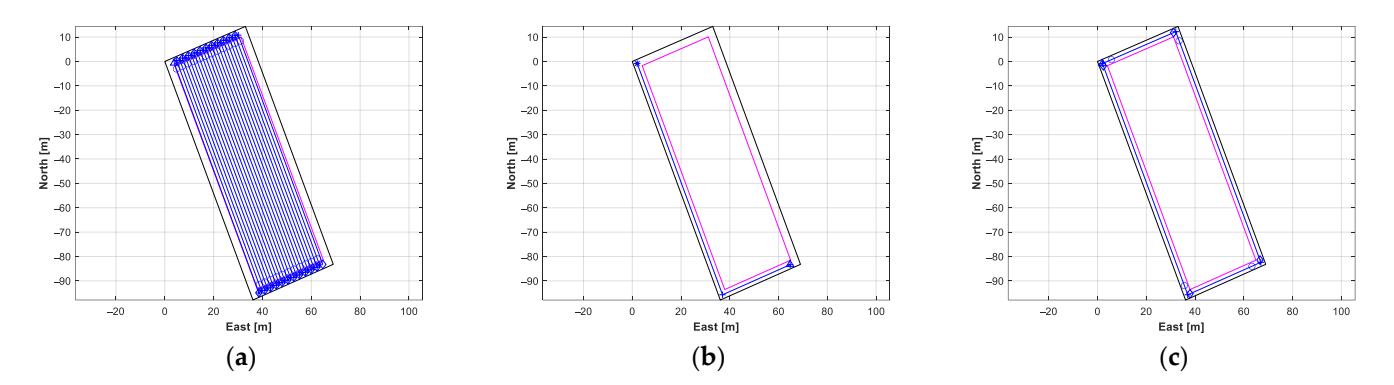


Figure 6. Waypoints for the rectangle-shaped field: external boundaries (black lines), internal boundaries (magenta line), autonomous driving path (blue lines), start waypoint (triangle), straight or turning waypoint (plus), work-starting waypoint (circle), work-ending waypoint (diamond), ending waypoint (star); (a) waypoints for ridge-forming work in the inner-field boundary; (b) waypoints for returning to the starting point; (c) waypoints for ridge-forming work in the headland area.

The waypoints for returning to near the first outer-field boundary point were generated as the shortest path starting from the last waypoint of the autonomous ridge-forming in the inner field to the vicinity of near the first outer-field boundary point, as shown in Figure 6b. The total number of generated waypoints is four, including one starting waypoint, two turning waypoints, and one ending waypoint, and the total length is

315.8 m. The waypoints for autonomous ridge-forming in the headland were generated so that ridges could be created by driving once along the field boundary line, from the last waypoint of the return waypoint, as shown in Figure 6c. The total number of generated waypoints is 13, including 1 starting waypoint, 4 turning waypoints, 4 work-starting waypoints, and 4 work-ending waypoints, and the total length is 735.6 m.

3.2.2. Trapezoid-Shaped Field

The geodetic coordinates of the trapezoid-shaped field boundary points for the test were entered clockwise from the northeast corner. The lengths of the four-line segments of the outer boundary of the field are approximately 34 m, 102 m, 21 m, and 103 m, clockwise from the first input point, respectively, and the area is approximately 2845 m². Figure 7a shows the result of generating the inner boundary of the field with the outer boundary of the field. The length of the four-line segments of the generated inner boundary are approximately 28 m, 96 m, 15 m, and 96 m. The generated MBR of the internal boundary to generate candidate sets consisting of line segments within the MBR is shown in Figure 7b.

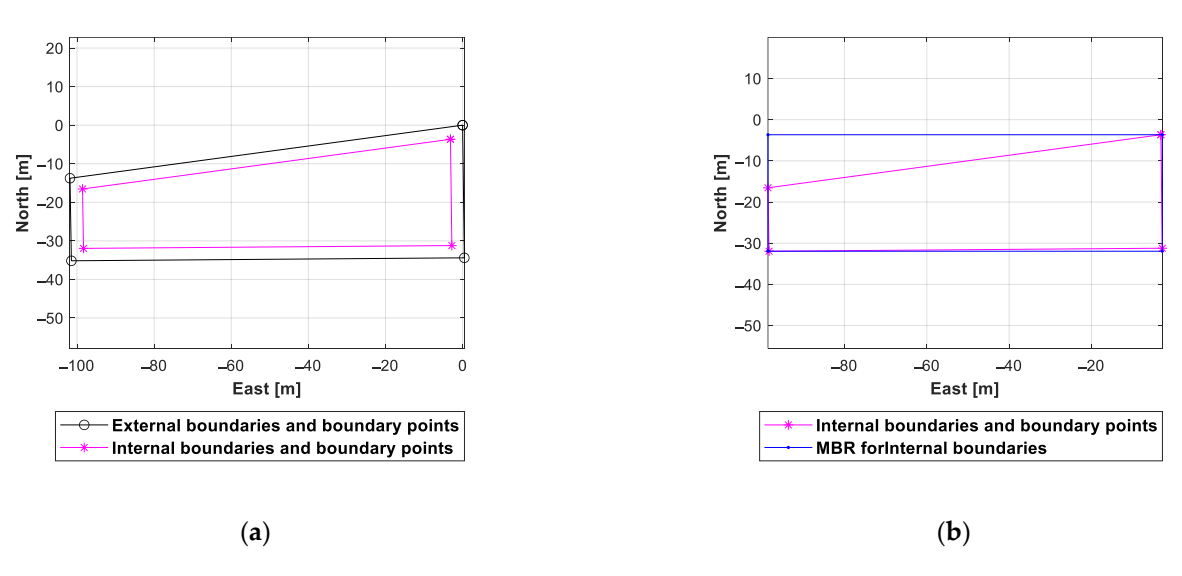


Figure 7. External and internal boundaries and MBR for the trapezoid-shaped field: (a) External and internal boundaries; (b) internal boundaries and MBR for internal boundaries.

The results of the generated working line segments in the inner-field boundary are shown in Figure 8a. A total of 74 working line segments in the inner-field boundary were generated in the north–south direction. The range of the lengths of the generated working line segments in the inner-field boundary is 15.4 m to 27.5 m, and the sum of the generated working line segments in the inner-field boundary is 1586.8 m. Figure 8b shows the result of the generated working line segments in the headland area. A total of four working line segments in the headland area were generated, since the shape of the field is a trapezoid. The lengths of the four-line segments of the generated working line segments in the headland area are approximately 26.0 m, 93.7 m, 13.4 m, and 94.5 m. The total area of the ridges created through the working line segments is 2177 m², so 77% of the field area is created as ridges.

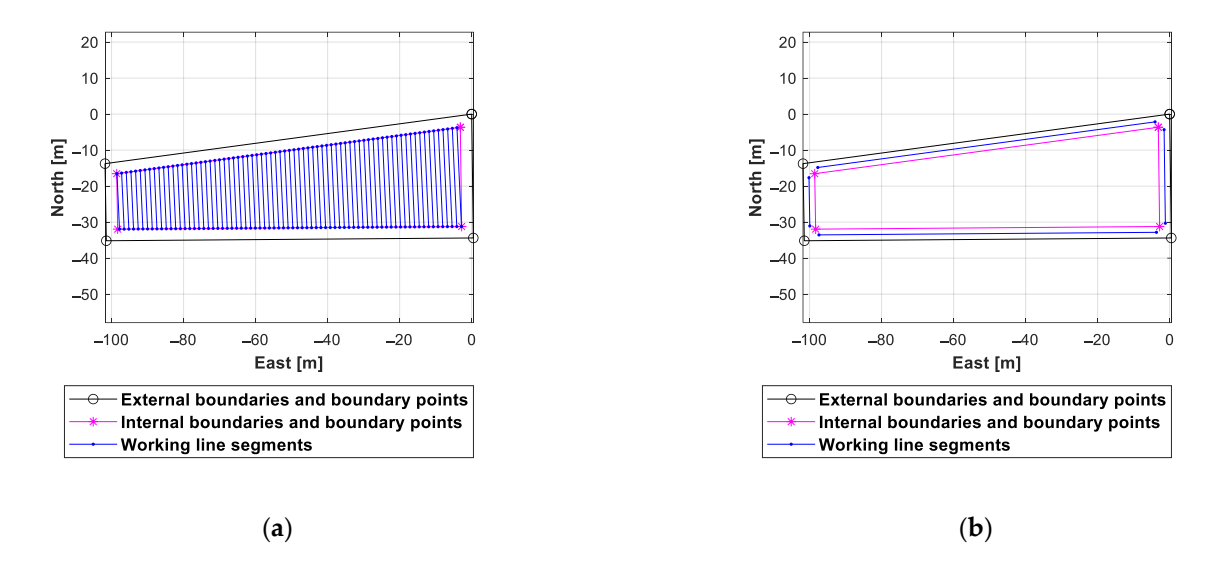


Figure 8. Working line segments for the trapezoid-shaped field: (a) working line segments in the inner-field boundary; (b) working line segments in the headland area.

The results of generating waypoints using working line segments based on the autonomous driving scenarios are shown in Figure 9. Waypoints for autonomous ridge-forming in the inner field were generated sequentially along the working line segments of the inner field that are closest in distance, starting near the first outer-field boundary point, as shown in Figure 9a. The total number of generated waypoints is 295, including 1 starting waypoint, 146 turning waypoints, 74 work-starting waypoints, and 74 work-ending waypoints, and the total length is 16,827.8 m. Figure 9b shows the results of the waypoints for returning to near the first outer-field boundary point. The waypoints were generated to reach near the first outer-field boundary point by the shortest distance within the headland area. Three waypoints consisting of one starting waypoint, one turning point, and one ending waypoint were generated. Figure 9c shows the result of the waypoints for autonomous ridge-forming in the headland. The total number of generated waypoints is 13, including 1 starting waypoint, 4 turning waypoints, 4 work-starting waypoints, and 4 work-ending waypoints, and the total length is 726.2 m.

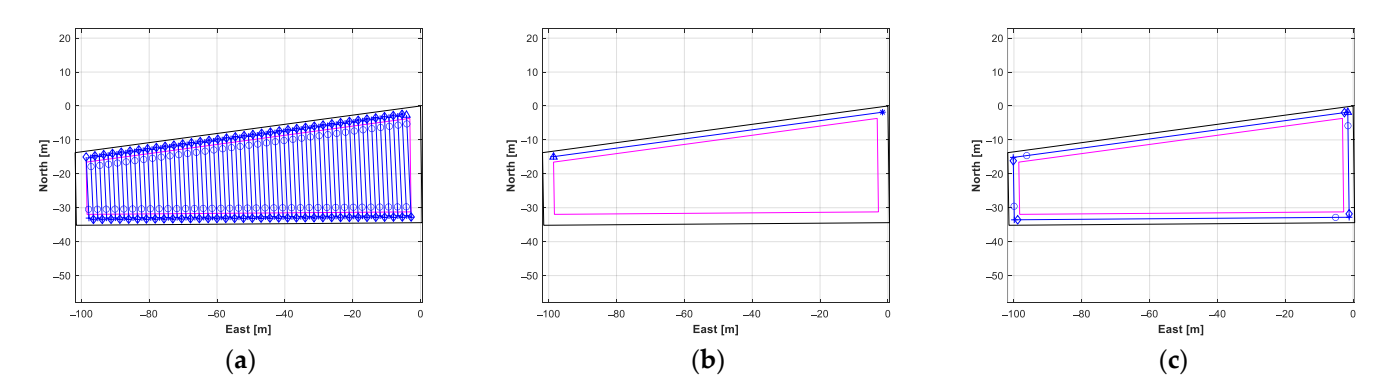


Figure 9. Waypoints for the trapezoid-shaped field: external boundaries (black lines), internal boundaries (magenta line), autonomous driving path (blue lines), start waypoint (triangle), straight or turning waypoint (plus), work-starting waypoint (circle), work-ending waypoint (diamond), ending waypoint (star); (a) waypoints for ridge-forming work in the inner-field boundary; (b) waypoints for returning to the starting point; (c) waypoints for ridge-forming work in the headland area.

3.2.3. Pentagon-Shaped Field

The geodetic coordinates of the pentagon-shaped field boundary points for the test were entered clockwise from the northwest corner. The lengths of the five-line segments

of the outer boundary of the field are approximately 89 m, 29 m, 86 m, 48 m, and 106 m, clockwise from the first input point, respectively, and the area is approximately 7873 m². The results of generating the inner boundary of the field using the coordinates of the input's external boundary vertices are shown in Figure 10a. The lengths of the five-line segments of the inner boundary were approximately 83 m, 25 m, 83 m, 43 m, and 99 m, respectively. Figure 10b shows the generated MBR of the internal boundary used to generate candidate sets consisting of line segments within the MBR.

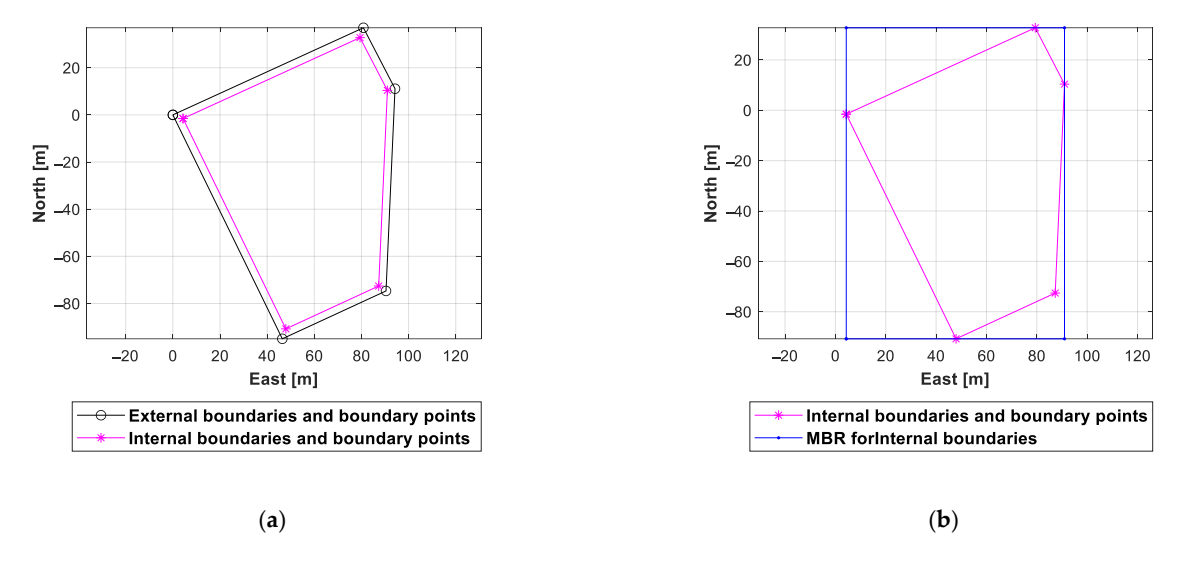


Figure 10. External and internal boundaries and MBR for the pentagon-shaped field: (a) External and internal boundaries; (b) internal boundaries and MBR for internal boundaries.

The results of the generated working line segments in the inner-field boundary and the headland area are shown in Figure 11a and Figure 11b, respectively. The number of generated working line segments in the inner-field boundary is 64. The range of the lengths of the generated working line segments in the inner-field boundary is 26.0 m to 99.3 m, and the sum of the generated working line segments in the inner-field boundary is 5228.2 m. A total of five working line segments in the headland area were generated along the field boundaries. The range of the lengths of the generated working line segments in the headland area was 22.2 m to 97.5 m, and the sum of the generated working line segments in the headland area was 320.7 m. The total area of the ridges created through the working line segments was 6658 m², so 85% of the field area was created as ridges.

For autonomous ridge-forming in the inner field, the result of the generated waypoints is shown in Figure 12a. A total of 255 waypoints were generated for autonomous ridge-forming in the inner field, and depending on the waypoint type, 1 starting waypoint, 126 turning waypoints, 64 work-starting waypoints, and 64 work-ending waypoints were generated. The total length of the autonomous driving path consisting of waypoints is 18,828.3 m. The waypoints for returning to near the first outer-field boundary point were generated as the shortest path starting from the last waypoint of the autonomous ridge-forming in the inner field to the vicinity of near the first outer-field boundary point, as shown in Figure 12b. The total number of generated waypoints is three, including one starting waypoint, one turning waypoints, and one ending waypoint, and the total length is 174.0 m. The waypoints for autonomous ridge-forming in the headland were generated, as shown in Figure 12c. The total number of generated waypoints is 16, including 1 starting waypoint, 5 turning waypoints, 5 work-starting waypoints, and 5 work-ending waypoints, and the total length is 1206.3 m.

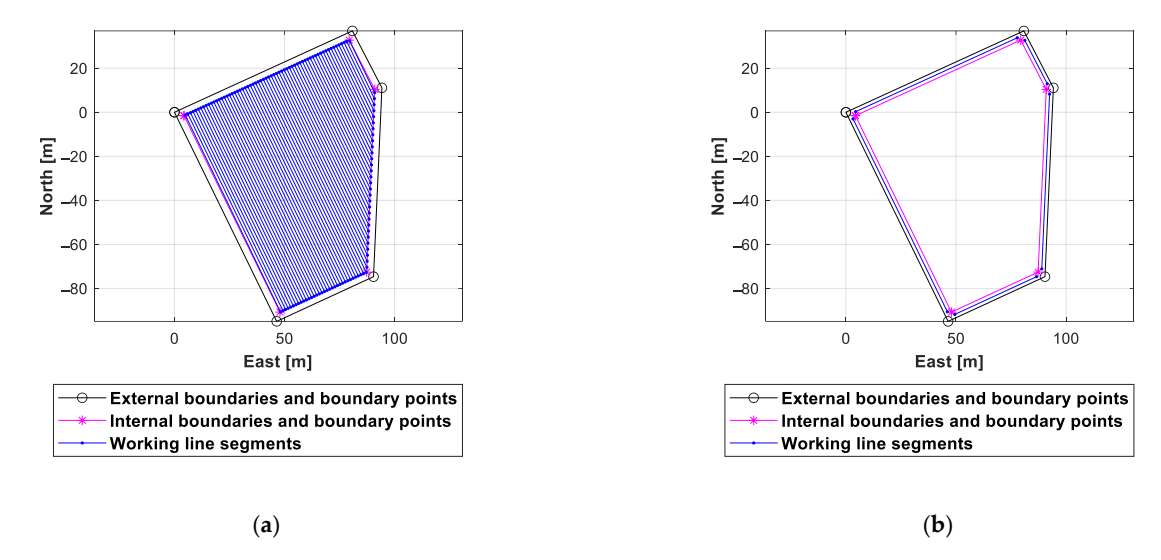


Figure 11. Working line segments for the pentagon-shaped field: (a) working line segments in the inner-field boundary; (b) working line segments in the headland area.

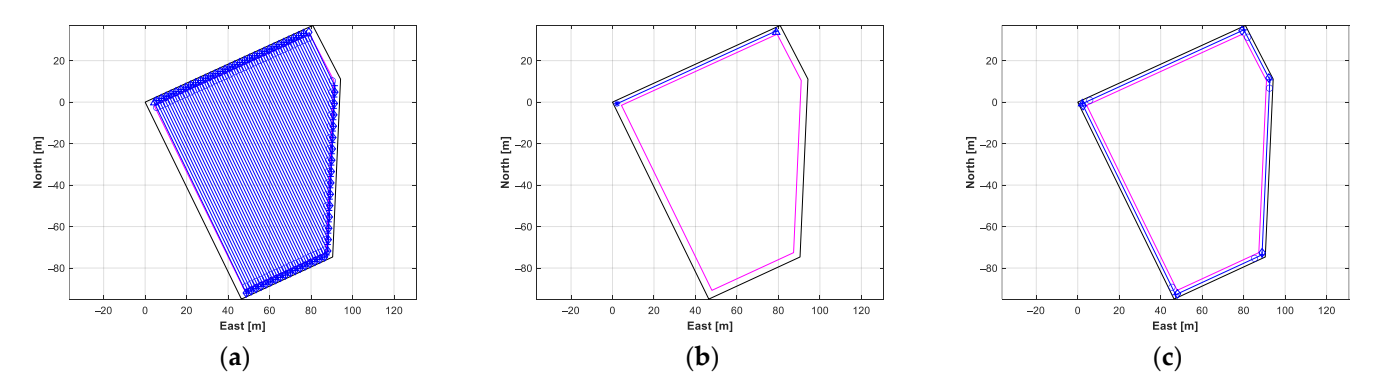


Figure 12. Waypoints for the pentagon-shaped field: external boundaries (black lines), internal boundaries (magenta line), autonomous driving path (blue lines), start waypoint (triangle), straight or turning waypoint (plus), work-starting waypoint (circle), work-ending waypoint (diamond), ending waypoint (star); (a) waypoints for ridge-forming work in the inner-field boundary; (b) waypoints for returning to the starting point; (c) waypoints for ridge-forming work in the headland area.

3.2.4. Hexagon-Shaped Field

The geodetic coordinates of the hexagon-shaped field boundary points for the test were entered clockwise from the southwest corner. The lengths of the six-line segments of the outer boundary of the field are approximately 70 m, 24 m, 27 m, 16 m, 43 m, and 39 m, clockwise from the first input point, respectively, and the area is approximately 2371 m². Figure 13a shows the result of generating the inner boundary of the field with the outer boundary of the field. The length of the six-line segments of the generated inner boundary are approximately 64 m, 17 m, 26 m, 16 m, 37 m, and 33 m. The generated MBR of the internal boundary to generate candidate sets consisting of line segments within the MBR is shown in Figure 13b.

The results of the generated working line segments in the inner-field boundary are shown in Figure 14a. A total of 50 working line segments in the inner-field boundary were generated in the west–east direction. The range of the lengths of the generated working line segments in the inner-field boundary is 17.4 m to 34.0 m, and the sum of the generated working line segments in the inner-field boundary is 1336.0 m. Figure 14b shows the results of the generated working line segments in the headland area. A total of six working line segments in the headland area were generated. The range of the length of the six-line segments of the generated working line segments in the headland area is 11.4 m to 62.2 m.

The total area of the ridges created through the working line segments is 1815 m², so 77% of the field area is created as ridges.

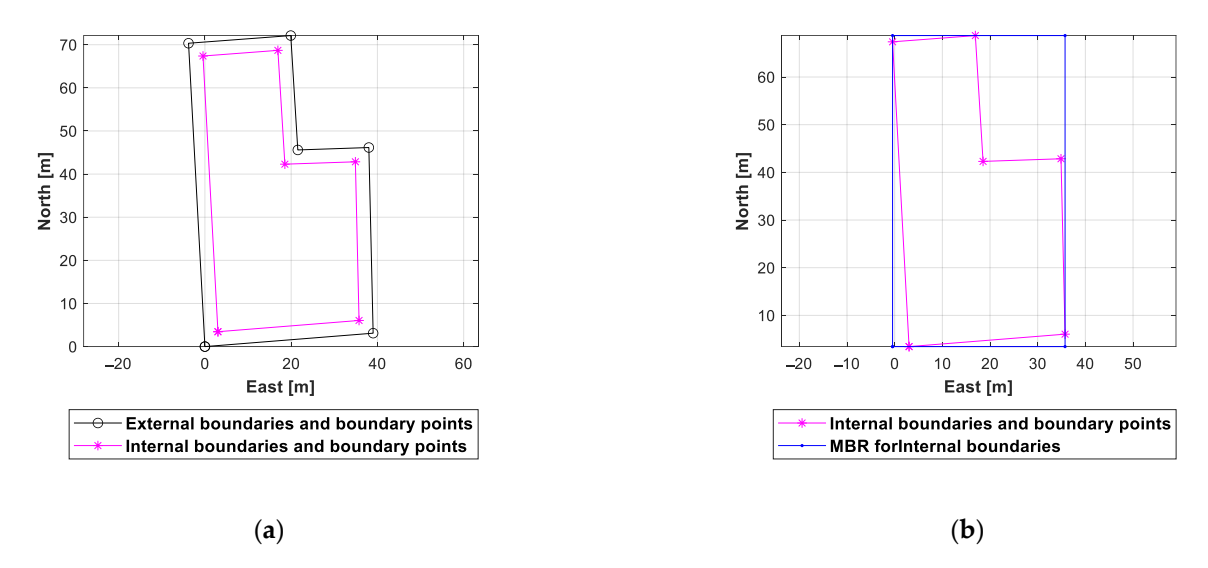


Figure 13. External and internal boundaries and MBR for the hexagon-shaped field: (a) External and internal boundaries; (b) internal boundaries and MBR for internal boundaries.

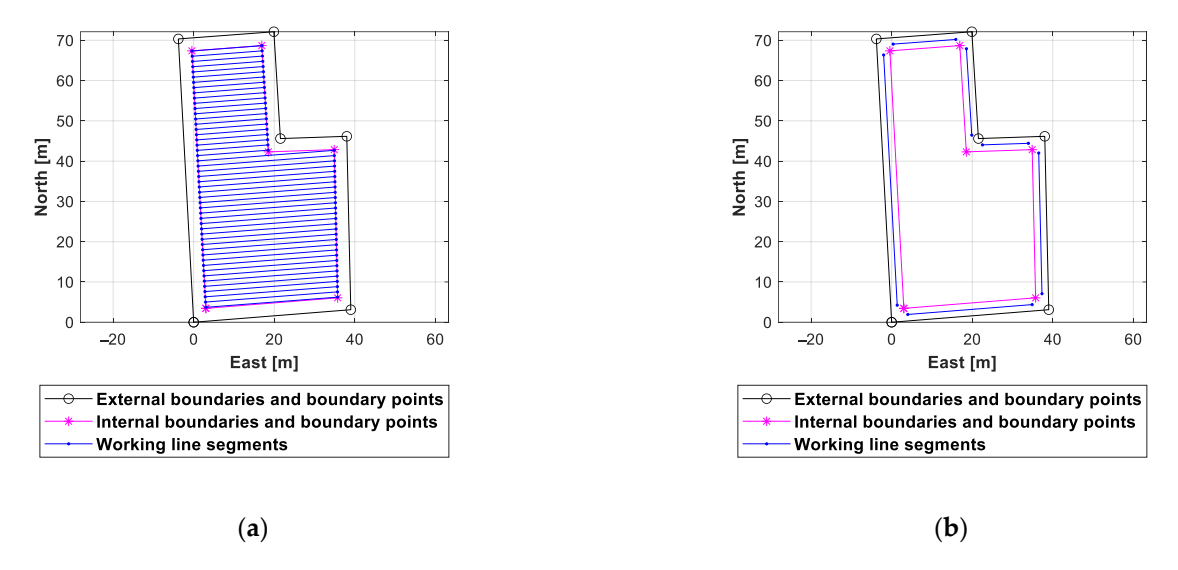


Figure 14. Working line segments for the hexagon-shaped field: (a) working line segments in the inner-field boundary; (b) working line segments in the headland area.

The results of generating waypoints using working line segments according to the autonomous driving scenarios are shown in Figure 15. Waypoints for autonomous ridge-forming in the inner field were generated sequentially along the working line segments of the inner field that are closest in distance, starting near the first outer-field boundary point, as shown in Figure 15a. The total number of generated waypoints is 199, including 1 starting waypoint, 98 turning waypoints, 50 work-starting waypoints, and 50 work-ending waypoints, and the total length is 8542.7 m. Figure 15b shows the results of the waypoints for returning to near the first outer-field boundary point. The waypoints were generated to reach near the first outer-field boundary point by the shortest distance within the headland area. The three waypoints consisted of one starting waypoint, one turning point, and one ending waypoint. Figure 15c shows the results of the waypoints for autonomous ridge-forming in the headland. The total number of generated waypoints is 19, including

1 starting waypoints, 6 turning waypoints, 6 work-starting waypoints, and 6 work-ending waypoints, and the total length is 859.5 m.

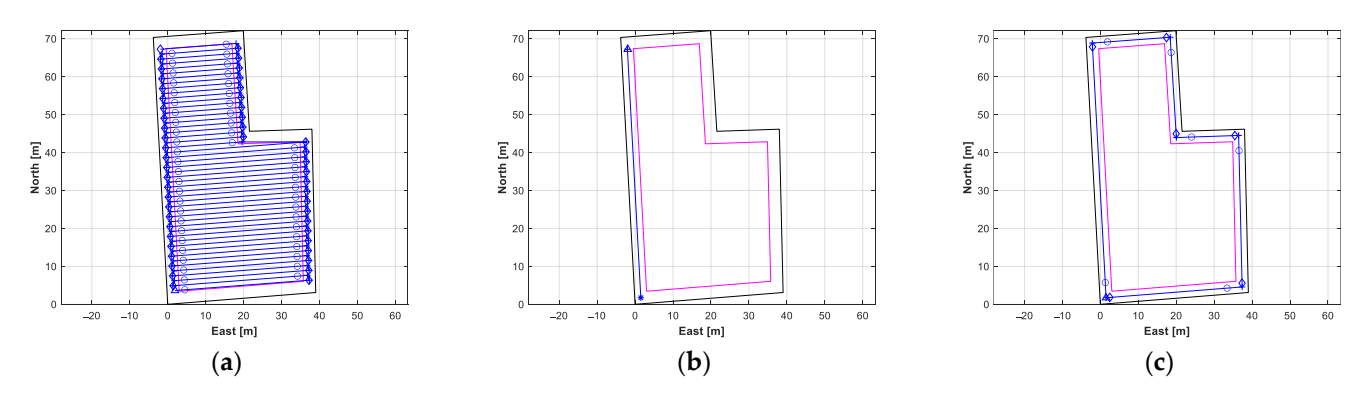


Figure 15. Waypoints for the hexagon-shaped field: external boundaries (black lines), internal boundaries (magenta line), autonomous driving path (blue lines), start waypoint (triangle), straight or turning waypoint (plus), work-starting waypoint (circle), work-ending waypoint (diamond), ending waypoint (star); (a) waypoints for ridge-forming work in the inner-field boundary; (b) waypoints for returning to the starting point; (c) waypoints for ridge-forming work in the headland area.

4. Discussion and Conclusions

In this paper, an autonomous driving path-generation algorithm was developed to generate waypoints for an autonomous driving crawler-type ridge-forming robot, using the geodetic coordinates of the field boundary points. The proposed algorithm defines outerand inner-field boundaries, generates working line segments in the inner-field boundary and the headland area, and then uses the working line segments to generate waypoints according to the autonomous driving scenario.

Three types of waypoints were generated based on the autonomous driving scenario: waypoints for autonomous ridge-forming in the inner field, waypoints for returning to the starting point in the headland area, and waypoints for autonomous ridge-forming in the headland area. To verify the proposed algorithm, waypoint generation tests were conducted based on four types of fields with different shapes (a rectangle, trapezoid, pentagon, and hexagon). The results for the three steps in the autonomous driving algorithm, a field boundary definition, working lines' generation, and waypoint generation, are summarized as follows.

Using the field boundary definition, the inner boundary of the field was generated appropriately by considering the shape of the field and the rotation radius of the robot. The working line segments in the inner-field boundary were generated by considering the width of the ridge, and the working line segments in the headland area were generated along the field boundaries. Lastly, the waypoints, which are the autonomous driving path, were appropriately generated sequentially, based on the shortest distance using the working line segments, so that the robot could drive and work continuously from the starting point. The test results confirm that the proposed algorithm can be used to generate an autonomous driving path for a crawler-type ridge-forming robot.

Based on the test results, the key elements discussed in this study are as follows. First, the proposed algorithm can efficiently generate a path using only the coordinates of field boundary points. The proposed algorithm has the advantage of reducing the time for acquiring data compared to methods [2–4] that generate routes using location data through manual driving and reducing the computation time compared to methods [5–10] that use complex geometric maps. The proposed algorithm has the advantage of increasing the working area because it generates a path considering the minimum turning section for a crawler-type ridge-forming robot. Therefore, the path can be generated more simply than

the path generation methods [12,13] for wheeled agricultural machinery without considering the turning, and the area of the headland area for the turning can also be minimized.

Future research will focus on the efficiency and practical applicability of the proposed algorithm. The details of future research are as follows. First, to verify the practical applicability of the proposed algorithm, we will conduct various field tests of autonomous ridge-forming using a crawler-type ridge-forming robot. Second, by implementing the existing path-generation algorithms, we will investigate the strengths and weaknesses of the proposed algorithm by deeper analysis and improve the algorithm. Third, we will conduct research to analyze the working method of the ridge-forming robot according to the shape of various fields and supplement the algorithm so that it can create a reliable path in fields of various shapes. Finally, to verify the efficiency of the proposed algorithm, we will conduct a comparative analysis of cases where a person performs the ridge-forming task directly and cases where the ridge-forming task is performed using autonomous driving.

Author Contributions: Conceptualization, J.-h.H. and C.-h.P.; Data curation, J.-h.H.; Formal analysis, J.-h.H.; Funding acquisition, C.-h.P.; Investigation, C.-h.P.; Methodology, J.-h.H.; Project administration, C.-h.P.; Resources, C.-h.P.; Software, J.-h.H.; Supervision, C.-h.P.; Validation, J.-h.H. and C.-h.P.; Visualization, J.-h.H.; Writing—original draft, J.-h.H.; Writing—review and editing, J.-h.H. and C.-h.P. All authors have read and agreed to the published version of the manuscript.

Funding: This work was supported by Korea Institute of Planning and Evaluation for Technology in Food, Agriculture, and Forestry (IPET) through the Open Field Smart Agriculture Technology Short-Term Advancement Program, funded by the Ministry of Agriculture, Food, and Rural Affairs (MAFRA) (RS-2022-IP322038).

Institutional Review Board Statement: Not applicable.

Informed Consent Statement: Not applicable.

Data Availability Statement: The original contributions presented in this study are included in the article. Further inquiries can be directed to the corresponding author.

Acknowledgments: This work was supported by Korea Institute of Planning and Evaluation for Technology in Food, Agriculture, and Forestry (IPET) through Open Field Smart Agriculture Technology Short-term Advancement Program, funded by Ministry of Agriculture, Food, and Rural Affairs (MAFRA) (RS-2022-IP322038).

Conflicts of Interest: The authors declare no conflicts of interest.

References

- Autonomous Tractors: Pros and Cons for Farmers in 2023. Available online: https://agtecher.com/autonomous-tractors-proscons (accessed on 28 October 2024).
- 2. Ünal, İ.; Topakci, M. Design of a Remote-controlled and GPS-guided Autonomous Robot for Precision Farming. *Int. J. Adv. Robot. Syst.* **2015**, *12*, 194. [CrossRef]
- 3. Han, J.-H.; Park, C.-H.; Jang, Y.Y.; Gu, J.D.; Kim, C.Y. Performance Evaluation of an Autonomously Driven Agricultural Vehicle in an Orchard Environment. *Sensors* 2022, 22, 114. [CrossRef] [PubMed]
- 4. Han, J.-H.; Park, C.-H.; Jang, Y.Y. Development of Location-Data-Based Orchard Passage Map Generation Method. *Sensors* **2024**, 24, 795. [CrossRef]
- 5. Palmer, R.J.; Wild, D.; Runtz, K. Improving the Efficiency of Field Operations. Biosyst. Eng. 2003, 84, 283–288. [CrossRef]
- 6. Taïx, M.; Souères, P.; Frayssinet, H.; Cordesses, L. Path planning for complete coverage with agricultural machines. In *Field and Service Robotics*; Springer: Berlin/Heidelberg, Germany, 2006; Volume 24, pp. 549–558.
- 7. Oksanen, T.; Visala, A. Path Planning Algorithms for Agricultural Machines. Agric. Eng. Int. CIGR J. Sci. Res. Dev. 2007, IX, 1–19.
- 8. Hameed, I.A.; Bochtis, D.D.; Sørensen, C.G.; Nøremark, M. Automated generation of guidance lines for operational field planning. *Biosyst. Eng.* **2010**, *107*, 294–306. [CrossRef]
- 9. Hameed, I.A.; La Cour-Harbo, A.; Osen, O.L. Side-to-side 3D coverage path planning approach for agricultural robots to minimize skip/overlap areas between swaths. *Robot. Auton. Syst.* **2016**, *76*, 36–45. [CrossRef]

10. Luck, J.D.; Pitla, S.K.; Shearer, S.A.; Mueller, T.G.; Dillon, C.R.; Fulton, J.P.; Higgins, S.F. Potential for pesticide and nutrient savings via map-based automatic boom section control of spray nozzles. *Comput. Electron. Agric.* **2010**, *70*, 19–26. [CrossRef]

- 11. Jeon, C.W.; Kim, H.J.; Yun, C.; Gang, M.; Han, X. An entry-exit path planner for an autonomous tractor in a paddy field. *Comput. Electron. Agric.* **2021**, 191, 106548. [CrossRef]
- 12. Han, X.; Kim, H.J.; Jeon, C.W.; Moon, H.C.; Kim, J.H.; Seo, I.H. Design and field testing of a polygonal paddy infield path planner for unmanned tillage operations. *Comput. Electron. Agric.* **2021**, *191*, 106567. [CrossRef]
- 13. Jeon, C.; Kim, H.; Yun, C.; Park, S.; Hwang, Y.; Han, X. Autonomous paddy field puddling and leveling operations based on full-coverage path generation and tracking. *Precis. Agric.* **2024**, 25, 235–256. [CrossRef]
- 14. Lee, K.; Choi, H.; Kim, J. Development of Path Generation and Algorithm for Autonomous Combine Harvester Using Dual GPS Antenna. *Sensors* **2023**, 23, 4944. [CrossRef] [PubMed]
- 15. Crisnapati, P.N.; Maneetham, D. Two-Dimensional Path Planning Platform for Autonomous Walk behind Hand Tractor. *Agriculture* **2022**, *12*, 2051. [CrossRef]

Disclaimer/Publisher's Note: The statements, opinions and data contained in all publications are solely those of the individual author(s) and contributor(s) and not of MDPI and/or the editor(s). MDPI and/or the editor(s) disclaim responsibility for any injury to people or property resulting from any ideas, methods, instructions or products referred to in the content.